Available online at www.sciencedirect.com
SCIENCE DIRECT®
Biomaterials 27 (2006) 2577–2586
Biomaterials
www.elsevier.com/locate/biomaterials

Biochemical consequences of alginate encapsulation: A NMR study of insulin-secreting cells

Nicholas E. Simpson[a], Samuel C. Grant[b,c], Lenita Gustavsson[d], Vilje-Mia Peltonen[d], Stephen J. Blackband[b,c,e], Ioannis Constantinidis[a,e,*]

[a]*Department of Medicine, University of Florida, Gainesville, FL 32610, USA*
[b]*Department of Neuroscience, University of Florida, Gainesville, FL, 32610*
[c]*McKnight Brain Institute, University of Florida, Gainesville, FL 32610, USA*
[d]*Royal Institute of Technology and the Royal Karolinska Medical and Surgical Institute, Stockholm, Sweden*
[e]*National High Magnetic Field Laboratory, Tallahassee, FL 32310, USA*

Received 31 August 2005; accepted 23 November 2005
Available online 20 December 2005

Abstract

In this study we explore the biochemical consequences of alginate encapsulation on βTC3 cells. ^{13}C NMR spectroscopy and isotopomer analysis were used to investigate the effects of encapsulation on several enzymatic processes associated with the TCA cycle. Our data show statistically significant differences in various enzymatic fluxes related to the TCA cycle and insulin secretion between monolayer and alginate-encapsulated cultures. The principal cause for these effects was the process of trypsinization. Embedding the trypsinized cells in alginate beads did not have a compounded effect on the enzymatic fluxes of entrapped cells. However, an additional small but statistically significant decrease in insulin secretion was measured in encapsulated cells. Finally, differences in either enzymatic fluxes or glucose consumption as a function of bead diameter were not observed. However, differences in T_2, assessed by ^{1}H NMR microimaging, were observed as a function of bead diameter, suggesting that smaller beads became more organized with time in culture, while larger beads displayed a looser organization.

Keywords: Alginate; Metabolism; ^{13}C NMR; Isotopomer

1. Introduction

Alginates are unbranched binary co-polymers of (1→4)-linked residues of β-D-mannuronic and α-L-guluronic acids of varying proportions, sequence, and molecular weight. Alginates have been used to encapsulate a variety of biological materials, including enzymes and cells of both microbial and mammalian origin. In tissue engineering, and particularly in the development of a bioartificial pancreas, alginates are commonly used to encapsulate islets [1–6] and transformed β-cells [7–12]. A layer of a polycation, such as poly-L-lysine, followed by an additional layer of alginate is used to coat the alginate matrix, generating a permselective membrane that permits the transport of low molecular weight nutrients and metabolites while excluding antibodies and cytotoxic cells; thus providing at least partial immunoprotection to the encapsulated cells. The physical properties of alginate hydrogels vary widely depending on their chemical composition and have been reported in numerous publications [13–19]. Despite this extensive literature, little is known about the biochemical consequences of alginate encapsulation on the encapsulated cells. Recently, we demonstrated the effects of alginate composition on the growth characteristics of encapsulated murine insulinoma cells [20–23]. Briefly, alginates rich in guluronic acid hindered growth and overall metabolic activity of the cells, while alginates rich in mannuronic acid did not affect either cell growth or metabolic activity. These effects were

*Corresponding author. Division of Endocrinology, Department of Medicine, PO Box 100226, University of Florida, Gainesville, FL 32610-0226, USA.
E-mail address: consti@medicine.ufl.edu (I. Constantinidis).

0142-9612/$ - see front matter © 2005 Elsevier Ltd. All rights reserved.
doi:10.1016/j.biomaterials.2005.11.042

attributed to the strength of the "egg-box" configuration [24] which varies depending upon the number and frequency of consecutive guluronic acid residues and the cation concentration at the time of gelation [15]. Although such studies illustrate the effect of alginate encapsulation on cell growth, they do not provide insight to the effects of encapsulation on specific biochemical processes and their relationship to insulin secretion. Understanding potential metabolic effects of encapsulation is critical in developing an optimum tissue-engineered pancreatic substitute.

Insulin secretion is an energy requiring process that is described by the "Fuel Hypothesis" [25–27]. While this concept is broadly accepted, there are aspects of metabolism that the model cannot adequately address. As a result, the importance of various enzymatic steps to secretion is still being investigated. For instance, Lu et al. [28] have recently utilized uniformly labeled ^{13}C glucose (U-^{13}C-glucose) and ^{13}C NMR spectroscopy and correlated the rate of pyruvate cycling to glucose-stimulated insulin secretion in INS-1 rat insulinoma cells, a previously undocumented relationship. Using similar techniques, Cline et al. [29] demonstrated a link between insulin secretion and enhanced anaplerosis to the TCA cycle through pyruvate carboxylase (PC). The effect of alginate encapsulation on such biochemical processes is not yet known. An earlier ^{13}C NMR study reported differences in glucose utilization between monolayer and alginate-entrapped cultures of βTC3 mouse insulinoma cells [9]. It was concluded that cells encapsulated in 1 mm alginate beads (at a density of 7×10^7 cells/ml) produced higher quantities of labeled lactate and possessed reduced TCA cycle activity compared to monolayer cultures. This conclusion was attributed to the reduced oxygen concentration within the alginate beads as a consequence of the alginate matrix acting as a diffusion barrier. In concert with this observation is a report showing that alginate-encapsulated βTC3 cells consumed oxygen at a rate that was 25% less than cells grown as monolayers in culture flasks [30]. This statistically significant decrease was accompanied by a 12% reduction in insulin secretion that was deemed not to be statistically significant.

In this study we used βTC3 cells encapsulated in alginate beads of varying diameter to investigate the effects of encapsulation and bead diameter on TCA cycle flux and insulin secretion. This is the first study investigating the effects of encapsulation on specific biochemical processes and their correlation to insulin secretion.

2. Methods

2.1. Cell culture

βTC3 cells were obtained from the laboratory of Shimon Efrat, Albert Einstein College of Medicine, Bronx, NY. Cells were cultured as monolayers in DMEM (Mediatech, Herndon, VA) containing ~22 mM glucose and supplemented with 15% horse serum, 2.5% bovine serum, 1% penicillin–streptomycin, and L-glutamine to a final concentration of 6 mM (SIGMA, St. Louis, MO). Cultures were grown at 37 °C under humidified (5% CO_2/95% air) conditions.

2.2. Alginate encapsulation

An alginate with a 62% mannuronic acid content (LVM by FMC BioPolymer, Drammen, Norway) was used in this study. An isotonic 2% (w/v) alginate solution was prepared by dissolving powdered alginate in physiological saline (0.85% NaCl), a solution that aids in the creation of homogeneous gel beads [14]. βTC3 cells were harvested from monolayer cultures using 0.05% trypsin–EDTA (Sigma, St. Louis, MO) and suspended in the sodium alginate solution at a density of 3.5×10^7 cells/ml alginate. Viable cell counts prior to encapsulation were performed using the trypan blue (Sigma, St. Louis, MO) exclusion method and were found to be >95% viable in each instance. Alginate beads were generated with the aid of an electrostatic bead generator (Nisco, Basel, Switzerland) which drops size-regulated beads from a needle into a solution of 100 mM $CaCl_2$, thus cross-linking the alginate. Bead size can be regulated by altering any of the following parameters: (i) the voltage potential between the $CaCl_2$ solution and the needle; (ii) the distance between the needle and the $CaCl_2$ solution; and (iii) the diameter of the needle extruding the alginate/cell suspension [31]. For this study we regulated the bead diameter by using needles with different diameters and maintained the voltage and the distance between the needle and the $CaCl_2$ solution constant. The diameters of the three needles used in this study were: (i) 0.35 mm, (ii) 0.70 mm, and (iii) 1.1 mm. Cell-containing beads were placed in T-75 flasks, fed with fully supplemented DMEM, and positioned onto a platform rocker (Stovall, Greensboro, NC) within a 37 °C humidified incubator. The diameter of a random sampling of beads ($n = 12$/encapsulation) was measured using a Nikon inverted microscope equipped with a calibrated eyepiece shortly after the beads were transferred into the T-flask. Resultant bead diameters were as follows: (i) the 0.35 mm diameter needle yielded 0.46 ± 0.02 mm beads; (ii) the 0.70 mm diameter needle yielded 0.75 ± 0.03 mm beads; and (iii) the 1.1 mm diameter needle yielded 1.15 ± 0.16 mm beads. Beads were incubated overnight, and media samples were collected at the beginning and at the end of the incubation period (approximate duration of 20 h) to assess the glucose consumption rate (GCR) in the encapsulated cultures.

2.3. U-^{13}C-glucose exposure and perchloric acid extraction

Media were removed from the flasks and the beads were washed and then incubated for 1.5 h with a serum-free/sugar-free Dulbecco's phosphate-buffered saline (DPBS) solution to normalize all experiments to the same initial condition. The beads were then incubated for 4 h with a fully supplemented glucose-free DMEM medium containing 15 mM U-^{13}C-glucose (Cambridge Isotopes, Cambridge, MA). Media samples were collected at the beginning and 20 min into the 4 h incubation period to assess the rate of insulin secreted by the encapsulated cultures prior to extraction. The same incubation and sampling protocol was also used for the monolayer and freshly trypsinized culture studies.

Perchloric acid extracts of monolayer cultures were performed directly in the tissue culture flask by adding 0.5 N perchloric acid (8 ml per flask). Cells were scraped from the flask surface, pooled in a centrifuge tube, and the cell suspension was homogenized for approximately 1 min. After allowing the precipitated protein salts to settle by gravity for 1–2 min, the sample was centrifuged at 4000g for 5 min. The supernatant was collected and neutralized with KOH. It was further centrifuged at 4000g for 10 min, and the supernatant was collected, passed through a Chelex-100 column to remove metal ions, adjusted to pH 7.4, and lyophilized. A similar protocol was also used for the extracts of freshly trypsinized and alginate-encapsulated cells. For alginate beads and freshly trypsinized cells, an equivalent volume of perchloric acid (0.5 N) was added to a volume of beads or cell pellet, respectively, and the beads or cell pellet were homogenized for approximately 2 min. The sample was set aside for 3–4 min to allow the bead solids to settle by gravity. After this step, the

procedure was equivalent to that described above for monolayers. This protocol was performed at 4 °C.

Lyophilized samples were dissolved in approximately 450 μl of D_2O (Cambridge Isotopes, Cambridge, MA). In the event that precipitated salts were observed, the sample was centrifuged at 4000*g* for 5 min and the supernatant passed through a 0.2 μm filter to remove any additional particulates. Samples were then placed in a 5 mm diameter NMR tube. Extracts from monolayer cultures consisted of approximately 1.0×10^9 cells, while extracts from encapsulated cultures consisted of approximately 2.5×10^8 cells. Each monolayer extract was repeated once while bead extracts were repeated twice.

2.4. NMR spectroscopy and microimaging

^{13}C NMR spectra were acquired using a 5 mm broadband receiving coil in an 11.75 T vertical bore Bruker Avance-500 (Bruker, Billerica, MA). A small coaxial insert containing a 2% dioxane solution was used as a concentration and chemical shift reference. Some of the key ^{13}C acquisition parameters were: 30 kHz spectral width; 16,384 complex points per free induction decay (FID); 6 s relaxation delay; and 10,240 transients. Waltz ^{1}H decoupling was applied throughout the acquisition. Resonances were assigned to metabolites based on their chemical shifts relative to the dioxane resonance at 67.4 ppm. All spectra were processed with a 2 Hz exponential line broadening filter prior to Fourier transformation.

^{13}C NMR spectra were processed using a Lorentzian fitting algorithm (“Nuts” by Acorn Inc., Fremont, CA) to determine the areas under the isotopomer patterns of C2-, C3-, C4-, and C5-glutamate. Correction factors to account for relaxation and nuclear Overhauser effects were applied to the resultant glutamate areas. Isotopomer patterns were analyzed with the aid of the tcaCALC software developed by the University of Texas Southwestern Medical Center, Dallas, TX [32,33]. This public domain software uses algebraic equations that take into account the contributions of these multiplets and applies Monte-Carlo simulations and non-linear least square analysis to yield parameters that determine relative pathway fluxes and isotope labeling contribution. Various models of glucose metabolism were tested to determine the best fit.

The model that presents the best fit of the data is presented in Fig. 1. It describes the entrance of ^{13}C-labeled pyruvate to the TCA cycle through both pyruvate dehydrogenase and PC and also includes a second anaplerotic entrance along the TCA cycle and a pyruvate cycling pathway that originates at oxaloacetate. Although the source for the second anaplerotic entrance has not been definitively identified, we have recently presented evidence that aspartate may be involved [34].

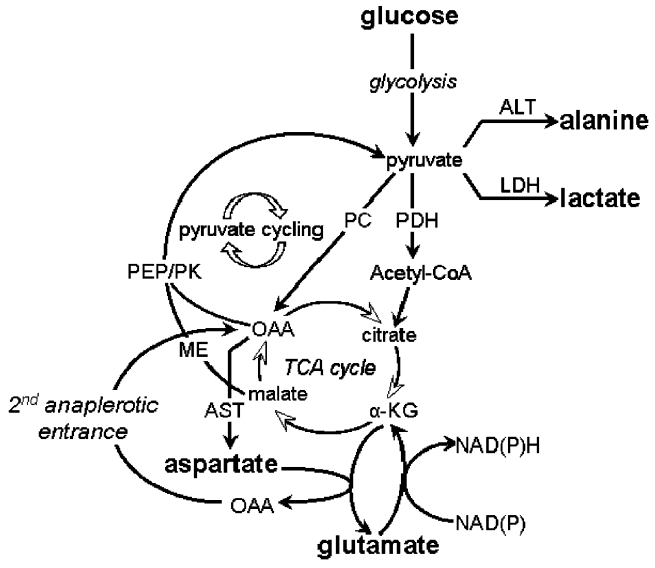

Fig. 1. Pathway of glucose metabolisms in β-cells: Metabolites in bold typeset are readily detectable in the ^{13}C NMR spectra.

Relative fluxes calculated by the isotopomeric analysis include the following, with the parameter as defined in the tcaCALC software in quotations: the relative flux through glycolysis upstream of pyruvate “LDH”; the % of acetyl-CoA derived from the pyruvate pool “PDH”; the flux through acetyl-CoA synthetase “ACS”; the ratio of pyruvate going through PC vs. pyruvate dehydrogenase “YPC”; the amount of non-PC anaplerotic carbon entrance to the TCA cycle “YS”; and the reformation of pyruvate from TCA cycle intermediates “PK”. The rates are relative to the TCA cycle (i.e., entrance via citrate synthase), defined as 1. Additionally, the fraction of ^{13}C-labeled pyruvate was also determined “LAC123”. The % anaplerosis is defined as the relative carbon entry from both anaplerotic pathways to the total carbon entering the TCA cycle, (YPC + YS)/(YPC + YS + 1)100. Pyruvate cycling is defined as the average between the YPC and PK fluxes [28,29].

^{1}H NMR images were acquired using a vertical 17.6-T 89-mm bore cryopumped magnet equipped with a Bruker Avance console and Micro2.5 gradients (maximum strength of 1000 mT/m). Beads immersed in DMEM were loaded into a capillary that was placed within a homebuilt solenoidal microcoil. Coupled with the high magnetic field, these small RF solenoids, which are susceptibility matched to reduce field perturbations, greatly improve the sensitivity of the NMR experiment [35]. Given the size of the alginate beads and the length of the microcoil, several beads were analyzed simultaneously. Images were acquired using a conventional spin-echo imaging sequence. In this sequence, a bipolar read-refocusing gradient pair was located after the second radio frequency pulse to minimize the effect of unintended water diffusion resulting from the read gradient [36]. For measurements of T_2, separate images were acquired at five echo times (TE = 15, 30, 45, 60, and 90 ms). T_2 (or spin–spin relaxation) is one of two fundamental NMR properties and it is defined as the interaction between neighboring nuclei with identical precessional frequencies but different magnetic quantum states. All other imaging parameters remained constant between images (NS = 4; TR = 1.5 s; MTX = 256 × 64; FOV = 5 × 1.3 mm; slice thickness = 0.06 mm). Diffusion weighted images were acquired at 5 diffusion weightings by incrementing the diffusion gradient strength (b value = 195, 507, 748, 977 and 1200 s/mm^2). All other imaging parameters remained constant between images (NS = 2; TR = 1.0 s; TE = 22 ms; Δ = 8.8 ms; δ = 2.4 ms; MTX = 256 × 128; FOV = 5 × 1.3 mm; slice thickness = 0.06 mm). The nominal pixel resolution of both T_2 and diffusion weighted images was 20 × 20 × 60 μm. Quantification of T_2 relaxation and apparent diffusion coefficient (ADC) was performed based on a region of interest (ROI) analysis. ADC is a measure of water diffusion. It is an apparent and not a true diffusion coefficient, determined from NMR images acquired with a pulse sequence sensitive to the motion of water. Circular ROIs encompassing the entire bead and the center of the bead were generated and the average signal intensity over the entire ROI was measured. Based on these measurements, the T_2 relaxation time and the ADC were calculated.

2.5. Analytical techniques

Glucose concentration in the culture medium was determined using a VITROS DT60II bioanalyzer (Ortho-Clinical Diagnostics, Rochester, NY). Insulin concentration in the culture medium was determined by a commercially available EIA kit (LINCO, St. Charles, MO) measured on a Synergy HT platereader (Bio-Tek, Winooski, VT), and the rate of insulin release over the 20 min period was calculated. Calculations of GCR or insulin secretion rate (ISR) were based on the change in the amount of glucose or insulin (amount = volume × concentration) between time points, divided by the corresponding time period. These rates were normalized to 10^5 cells at the onset of the experiment.

2.6. Histology

Alginate beads were fixed with a mixture of 1% glutaraldehyde and 2% paraformaldehyde (Sigma, St. Louis, MO) in Tyrode’s Buffer (pH 7.2).

After 20 min of fixing time, the beads were rinsed three times in 70% ethanol, and stored in 70% ethanol at 4 °C. The samples were embedded in paraffin, sliced, and stained with Hematoxylin and Eosin (H/E).

2.7. Statistical analysis

The statistical significance in the difference between groups within a set of data (e.g., monolayer versus encapsulated cells or small versus large beads) was determined with a Student's *t*-test (two-tailed) for independent samples.

3. Results

^{1}H-decoupled ^{13}C NMR spectra were acquired from perchloric acid extractions of βTC3 monolayer, freshly trypsinized, and alginate-entrapped cultures. Fig. 2 shows representative ^{13}C NMR spectra from monolayer and bead extracts. Four hour incubation with U-^{13}C-glucose labeled media yields resonances from a variety of metabolites. Table 1 lists the ^{13}C detected carbons and their corresponding assignments. Simulating resonances of the monolayer spectra to a Lorentzian fitting routine, we deduce that the most prevalent metabolite produced by glucose-consuming βTC3 cells is lactate. This implies that much of the pyruvate in βTC3 cells is metabolized to produce lactate (through lactate dehydrogenase) rather than converted to products that enter the TCA cycle. The second most prevalent labeled metabolite is glutamate, an amino acid synthesized directly from the TCA cycle, followed by alanine, aspartate, and glycine. In addition, the amino acid serine, as well as TCA cycle intermediates malate and citrate, and glycolytic intermediates fructose-6-phosphate and fructose-1,6-diphosphate are detected. A small resonance assigned to (1–4)-glycogen is also detected as well as a few resonances as yet unassigned.

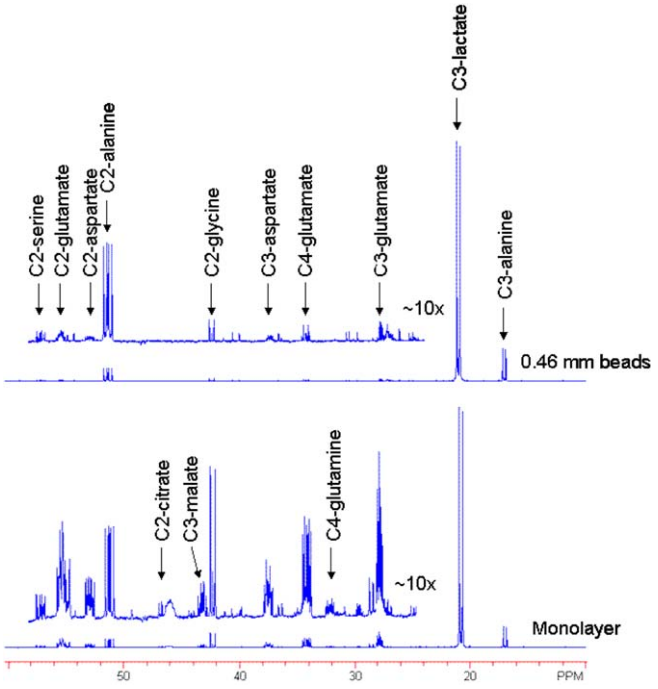

Fig. 2. Representative proton-decoupled ^{13}C-NMR spectra obtained from extracts of βTC3 monolayer and alginate-encapsulated cultures exposed to 15 mM uniformly labeled ^{13}C-glucose. The corresponding resonance assignments are indicated on the figure.

Table 1
^{13}C NMR detectable metabolites based on perchloric acid extracts of βTC3 cells incubated with U-^{13}C-glucose for 4 h

Metabolite carbon	Chemical shift (ppm)	Effect of encapsulation
Alanine-C3	17	Increase
Lactate-C3	21	Increase
Glutamine-C3	26.5	Decrease
Glutamate-C3	27.5	Decrease
Glutamine-C4	32	Decrease
Glutamate-C4	34	Decrease
Aspartate-C3	37.5	Decrease
Glycine-C2	42.5	Decrease
Citrate-Mg^{+2}-C2	45.5	Decrease
Citrate-C2	46.8	Decrease
Alanine-C2	51.5	Increase
Aspartate-C2	53	Decrease
Glutamine-C2	55	Decrease
Glutamate-C2	55.5	Decrease
Serine-C2	57	Decrease
Fructose-1,6-diphosphate-C6	64.4	Decrease
Fructose-6-phosphate-C6	66	Absent
Lactate-C2	69.5	Increase
Fructose-1,6-diphosphate-C3	82.5	Decrease
Fructose-1,6-diphosphate-C5	84	Decrease
Unassigned	87.5	Absent
Unassigned	89.5	Absent
Fructose-6-phosphate-C3	90.2	Absent
(1–4)Glycogen-C1	100.5	Unaffected
Fructose-1,6-diphosphate-C2	103	Decrease
Unassigned	170	Increase
Glycine-C1	173.5	Decrease
Serine-C1	173.5	Decrease
Aspartate-C4	175.5	Decrease
Glutamine-C1	176	Decrease
Glutamate-C1	176	Decrease
Alanine-C1	176.5	Increase
Citrate-C1 and C5	180	Decrease
Glutamate-C5	182	Decrease
Lactate-C1	183.3	Increase

Alginate encapsulation has a dramatic effect on the appearance of the ^{13}C NMR spectrum (see Table 1). Whereas lactate and alanine resonances are elevated with encapsulation, all other metabolites, including glutamate, aspartate, and TCA cycle intermediates are decreased. This apparent reduction in TCA cycle activity and concomitant elevation in lactate and alanine corroborates our earlier report [9]. It is important to note that there are no discernable bead size-dependent differences in spectra profile.

Table 2
A list of relative fluxes determined by simulating glutamate isotopomer patterns with tcaCALC for the five set of extracts examined in this study

	Monolayer	Freshly trypsinized	0.46 mm beads	0.75 mm beads	1.15 mm beads	All beads
^{13}C labeled pyruvate	0.70±0.08	0.84±0.12	0.64±0.11	0.69±0.22	0.67±0.15	0.67±0.13
Glycolysis	2.15±0.01	1.01±0.22	0.91±0.08	0.91±0.16	1.01±0.06	0.94±0.09
p-values		0.0176	0.0022	0.0080	0.0015	<0.0001
Fatty acid metabolism	0.14±0.16	0.04±0.02	0.29±0.16	0.33±0.16	0.21±0.02	0.27±0.15
PDH	0.86±0.16	0.96±0.02	0.71±0.16	0.67±0.31	0.79±0.02	0.73±0.17
PC	2.18±0.05	0.96±0.31	0.73±0.15	0.65±0.28	0.72±0.06	0.70±0.15
p-values		0.0322	0.0056	0.0173	0.0014	<0.0001
Pyruvate cycling	0.89±0.20	0.92±0.11	0.57±0.14	0.42±0.13	0.50±0.02	0.50±0.11
2nd anaplerotic entrance	0.14±0.10	0.37±0.06	0.44±0.04	0.36±0.01	0.43±0.09	0.37±0.06
p-values		0.1113	0.0568	0.0897	0.0873	0.0023
% anaplerosis	69.9±0.5	56.9±4.7	53.9±3.9	50.0±6.7	53.5±3.2	52.5±4.2
p-values		0.0592	0.0287	0.0530	0.0187	0.0015
Sum of squares	0.003±0.001	0.019±0.016	0.015±0.009	0.018±0.007	0.019±0.011	
C3/C4% error	1.78±0.25	6.77±6.65	1.90±1.16	1.10±1.41	3.24±4.47	

The column "all beads" represent values averaged over all encapsulations independent of bead diameter. *p*-values are presented for parameters that show statistically significant differences with encapsulation. The rows "sum of squares" and "C3/C4% error" represent statistical measures representing the goodness of the model.

Using the fitted areas of the individual multiplet patterns of each glutamate carbon resonance as the input to the tcaCALC software, relative metabolic fluxes for the model described in Fig. 1 were determined. Table 2 lists the value of these fluxes and how they are affected by bead diameter and trypsinization. The model fit the data well (low residual difference between the model-generated results and the measured isotopomeric fraction data) with an average glutamate C3/C4% error much less than 5%. Our data show that encapsulation causes a statistically significant reduction in the relative flux through glycolysis and PC, with an increase in the entrance to the TCA cycle through the second non-PC anaplerotic pathway.

Fig. 3 shows the effect of encapsulation on insulin secretion by the monolayer, freshly trypsinized, and alginate-encapsulated cultures over a 20 min period. These data show that insulin secretion is significantly reduced by the trypsinization process, corroborating our earlier report [9]. Alginate encapsulation caused an additional reduction of insulin secretion that was statistically significant. Correlations emerged between the insulin secretion (measured from each of these cultures prior to extraction) and the following relative metabolic fluxes (determined by isotopomer analysis of the ^{13}C NMR spectra): (a) the relative flux through glycolysis upstream of pyruvate; (b) the relative flux through PC; (c) the relative flux through the second anaplerotic entrance and (d) the percent of total anaplerosis to the TCA cycle. These correlations are shown in Fig. 4.

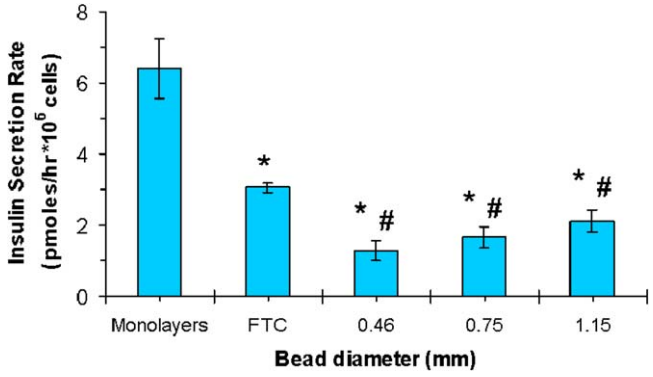

Fig. 3. Insulin secretion rates for monolayer, freshly trypsinized (FTC) and encapsulated cultures. * represent statistical significant differences ($p<0.05$) against monolayer cultures while the pound symbols represent statistical significance against freshly trypsinized cells.

It is important to note that we did not observe any statistically significant differences in modeled parameters of metabolism as a function of bead diameter. This is further corroborated by the lack of a significant difference in the rate of glucose consumption by the three encapsulation groups. The glucose consumption for beads with a 0.46 mm diameter was 7.69 ± 1.65 nmoles/h $\times 10^5$ cells, while for beads with 0.75 mm and 1.15 mm diameters were 6.60 ± 0.91 and 7.04 ± 0.75 nmoles/h $\times 10^5$ cells, respectively. This observation was unexpected given that the diffusional barrier imposed by alginate increases with bead diameter. Thus, cells at the center of larger beads experience more adverse conditions than cells at the center

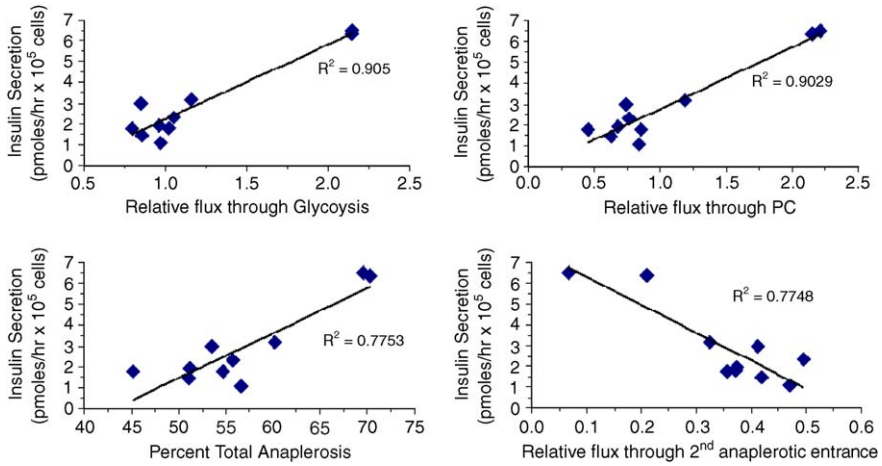

Fig. 4. Correlations of insulin secretion with metabolic fluxes determined by isotopomeric analysis. Points presented on these graphs represent all samples examined in this study. The solid line and the R^2 values are determined using the best fit of the data based on a linear least square analysis.

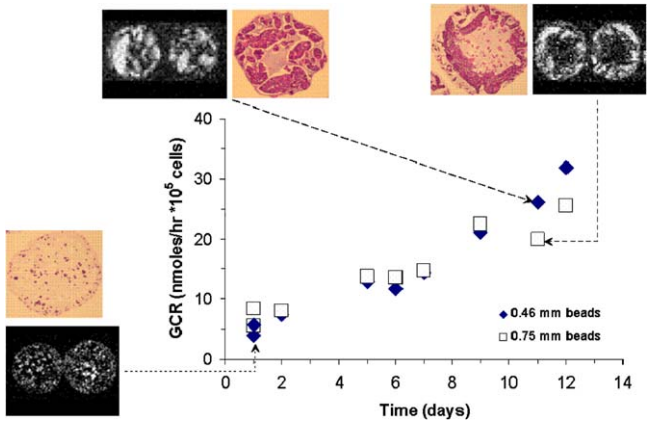

Fig. 5. Temporal changes in glucose consumption rate (GCR) by small (0.46 mm) and medium (0.75 mm) size beads. ^{1}H MR microimages and H/E stained cross-sections or representative beads show the differences in cell growth between the two different bead sizes.

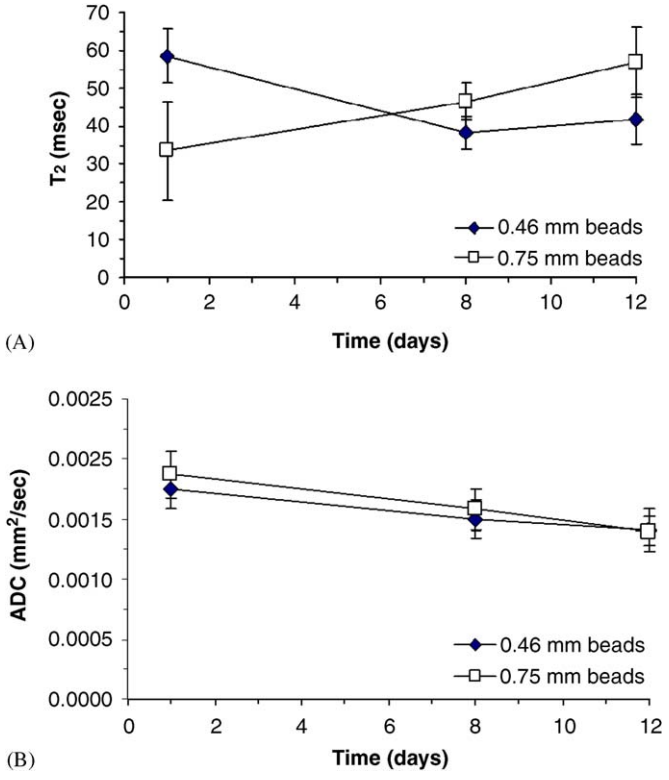

Fig. 6. Temporal changes in T_2 (Panel A) and the apparent diffusion coefficient (ADC) (Panel B) for 0.46 and 0.75 mm beads containing βTC3 cells. The error bars represent standard deviations of the measurements.

of smaller beads. To assess whether bead size may have long-term effects in the metabolic activity of the cells, cultures from 0.46 and 0.75 mm beads were cultured for 2 weeks. The GCR was measured periodically, and its temporal change assessed. In addition, T_2 and diffusion weighted MR microimages were obtained from individual beads on days 1, 8, and 12. Both GCR and imaging data are shown in Fig. 5. The data show that GCR increases linearly with time in culture, but there are no significant differences between the two bead sizes. ^{1}H NMR microimages show that cells encapsulated in larger beads grew in clusters located at the periphery of the bead creating an *o*-ring pattern, while cells encapsulated in smaller beads grew in clusters throughout the bead. These growth patterns were validated by histology cross-sections stained with hematoxylin/eosin. ROI analysis of the T_2 and diffusion weighted images reveal significant differences in T_2 and ADC with time in culture and between the two bead sizes. Figs. 6A and B depict temporal changes in T_2 and ADC, respectively, for beads with 0.46 and 0.75 mm diameter. The data show that for beads with an initial bead diameter of 0.46 mm, T_2 decreased with time, reaching statistical significance on both days 8 and 12. There was no statistical difference between the measurements made on days 8 and 12. Conversely, for beads with an initial bead diameter of 0.75 mm, T_2 increased with time, reaching statistical significance on Day 12. Furthermore, statistically significant differences were observed on all three time points between small and large beads. ADC measurements decreased with time in culture regardless of

the initial bead diameter reaching statistical significant on both days 8 and 12. However, there were no statistical differences between the two bead sizes.

4. Discussion

Understanding the effects of encapsulation on the metabolic and secretory mechanisms of cells is critical to the design of an optimum bioartificial pancreas. Our data demonstrate several significant differences between cells cultured as monolayers and cells cultured within alginate beads. The first notable difference is the increase in lactate and alanine production and the concomitant decrease in TCA cycle activity with alginate encapsulation. This observation supports earlier ^{13}C NMR data [9] attributed to the reduced oxygen availability in an encapsulated environment. The fact that insulin-secreting βTC3 cells metabolize pyruvate primarily through lactate dehydrogenase to produce lactate is common for transformed cell lines [37]. However, it does not necessarily reflect the metabolic propensity of islets [38] or other insulin-secreting cell lines such as the INS-1 (unpublished data).

Our observation that increasing the diameter of the beads from 0.46 to 1.15 mm did not affect either the metabolic or the secretory activity of the cells was unexpected. Given that the oxygen concentration at the center of a larger bead is lower than at the center of a smaller bead, one would expect that smaller beads would display more (and perhaps different) TCA cycle activity than larger beads. However, a computer modeling analysis of alginate-encapsulated βTC3 cells has shown that in fresh preparations of encapsulated cells, assuming 100% viability and uniform distribution of cells throughout the bead, the oxygen tension at the center of 1 mm beads containing 3×10^7 cells/ml alginate and maintained in media saturated with air is approximately 120 mmHg [39]. This value is well above the thresholds of 25 and 7 mmHg which have been shown to affect glucose metabolism and insulin secretion, respectively, in βTC3 monolayer cultures [40]. Because the extractions in this study took place within 24 h of encapsulation, entrapped cells were still uniformly distributed in the beads as they did not have the time to replicate and rearrange, a process known to exacerbate nutrient gradients along the bead radius and lead to the generation of necrotic cores in large beads (Fig. 5). Thus, the absence of significant biochemical differences between bead sizes is due to the presence of an adequate nutrient supply within the microcapsule environment. Following the same argument, the statistically significant difference in insulin secretion between monolayer and entrapped cultures cannot be attributed to oxygen limitations. A possible explanation is that the threshold of 7 mmHg, mentioned above, may not be valid for encapsulated conditions. Papas et al. [41,42] in a series of two papers, examined the effects of hypoxia on insulin secretion by alginate-encapsulated βTC3 cells. These studies demonstrated that insulin secretion was affected at oxygen conditions above 7 mmHg, although a threshold was not defined. It can be argued that because experiments reported in this study were conducted at the same glucose concentration, changes in insulin secretion do not reflect changes in enzymatic processes related to the "fuel hypothesis" [26,27,43,44]. Thus, these observations may be attributed to a physical property of the construct such as binding of insulin to alginate. However, this is not supported by data available in the literature [45,46]. Another explanation for the observed differences between monolayer and entrapped cultures is the effect of trypsinization on the cells. Mukundan et al. [30] demonstrated that for βTC3 cells the rate of oxygen consumption was statistically reduced in freshly trypsinized and alginate-encapsulated cultures compared to monolayer cultures. However, there was no statistical difference between freshly trypsinized cells and cells encapsulated in alginate beads. Our present data corroborate this observation and suggest that the principal cause in the reduction of insulin secretion by encapsulated cultures is the trypsinization step. Allowing encapsulated cells to recover from the effects of trypsin for a few days may provide a clue as to whether these effects are reversible. However, cultures of APA-encapsulated βTC3 cells maintained in vitro for 30 days did not demonstrate an increase in insulin secretion, unless accompanied by significant cell growth [47]. Thus, the observed effects do not appear to be transient, and extracts performed on encapsulated cultures at times beyond the first 24 h are impractical because they are confounded by a heterogeneous cell population generated as a consequence of steep gradients in dissolved oxygen concentration developed during cell growth. Furthermore, it is doubtful that liquefying the central alginate matrix with citrate, a practice commonly used with islet encapsulation, will reverse the effects of trypsinization.

Despite the lack of metabolic or secretory differences with bead size, MR microimages and histology cross-sections showed a notable difference in the pattern of cell growth. Since both bead preparations were cultured under the same environmental conditions, the oxygen tension at the surface of the beads will dictate the distance from the surface of the bead within which viable cells can be maintained. This thickness is independent of bead diameter, and it has been demonstrated that under well-oxygenated conditions, cell viability can be maintained only within 150–200 μm from the source of oxygen [48,49]. Because the viable cell layer in the larger beads is approximately 200 μm, a distance equivalent to the diameter of the smaller beads (230 μm), we conclude that the observed difference does not represent a true change in growth pattern. Thus, the growth pattern in the smaller beads is equivalent to the growth pattern within the viable rim of the larger beads. However, quantitative analysis of T_2 shows statistical differences between 0.46 and 0.75 mm beads. Specifically, smaller beads demonstrate a decreasing T_2 with time in culture suggesting that the constructs become more organized throughout their entire volume as

a result of cell growth and concomitant alterations of the alginate matrix. Conversely, larger beads demonstrate an increasing T_2 with time in culture, which betrays a looser organization likely due to an overall swelling of the alginate and the increased cell death in the core of the larger bead. Importantly, the progressive decrease in ADC with time is consistent in both construct sizes, which is attributed to cell proliferation and the increasing presence of restrictive barriers (e.g. cell membranes) to the translational motion of water.

To assess changes in TCA cycle flux as a function of encapsulation, several models of glucose metabolism were tested (results of two models are described below). The model with two anaplerotic entrances to the TCA cycle (shown in Fig. 1) demonstrated the best fit for all data acquired in this study. This model showed that with encapsulation, there are strong statistically significant reductions in the relative fluxes through glycolysis (upstream of pyruvate) and through PC, and a reduction in the percent of total anaplerosis to the TCA cycle. The correlation between insulin secretion and relative flux through glycolysis corroborates existing data suggesting that early steps in glycolysis are important triggers of insulin secretion, while the importance of anaplerosis to insulin secretion has also been demonstrated [50]. For encapsulated cells the reduction in the flux through glycolysis is counterintuitive, because the production of lactate increases with encapsulation. This disparity is explained by the difference in the fate of pyruvate between monolayer and encapsulated cultures, not the overall production of lactate. Although lactate is the dominant product under both culture conditions, in monolayer cultures a large portion of pyruvate enters the TCA cycle, while in encapsulated cultures only a small fraction of pyruvate enters the TCA cycle. This explanation is supported by our ^{13}C data showing that the relative flux through PC, as well as all TCA cycle intermediates and TCA cycle derived amino acids, are reduced for all encapsulated cultures.

Contrary to these reductions, an increase in the relative flux through the second anaplerotic entrance was observed with encapsulation. Although this increase did not reach statistical significance when comparing individual bead size versus monolayers, it achieved statistical significance when all encapsulation data were pooled together. This correlation is contrary to the correlation observed for INS-1 and R7T1 cells cultured as monolayers and examined under different glucose concentrations or media complexity [34]. Under similar culture conditions, βTC3 and βTCtet cells did not demonstrate a significant correlation between insulin secretion and the relative flux of the second anaplerotic entrance. This discrepancy is attributed to both cell-line-dependent effects and the process of encapsulation. It is important to point out that metabolic flux data obtained from freshly trypsinized cells were significantly different from monolayer cells but not statistically different from encapsulated cells. This observation correlates with the insulin secretion measurements showing that trypsinization had a significant effect on the cells.

In addition to this model, we fitted our data to a recently proposed model describing the presence of two distinct, and to a large extent, non-communicating pyruvate pools [28]. The first pool is the terminal end of glycolysis and feeds pyruvate into the TCA cycle through PDH. The second pyruvate pool is generated from carbons exiting the TCA cycle at malate and/or oxaloacetate and reentering the TCA cycle through PC. This model does not have a second (i.e., non-PC) anaplerotic entrance. Applying the two-pyruvate pool model to cellular extracts from various INS-1 clones, Lu et al. [28] demonstrated that flux through pyruvate cycling (i.e., carbon cycling between the TCA cycle and the second pyruvate pool) correlated to glucose stimulated insulin secretion. When applied to our data, the two-pyruvate pool model fit the majority, but not all, of our spectra with equal confidence as the model described in Fig. 1. However, the results on TCA cycle flux as a function of encapsulation were model-dependent. Specifically, metabolic parameters obtained from the two-pyruvate pool model showed that encapsulated cultures (when pooled) have a statistically significant reduction in the isotopic enrichment of both pyruvate pools and the relative flux through glycolysis compared to monolayer cultures. However, these observations were not statistically significant for all three bead sizes, nor was there a definite trend with bead size. The remaining modeled metabolic parameters were unaffected by encapsulation. It is also important to note that pyruvate cycling was not affected by encapsulation and thus did not correlate with insulin secretion. This is in contrast to the correlation found in INS-1 cells and presented by Lu et al. [28].

5. Conclusion

Overall, our data demonstrate that the process of alginate encapsulation affects certain enzymatic processes related to glucose utilization and consequently insulin secretion. However, the principal culprit of this effect is the trypsinization step. It remains to be determined whether it can be ameliorated by other cell-detachment techniques. Our data also show that the metabolic activity and growth pattern of encapsulated cells are not affected by the size of the capsules although there are some size dependent differences in the organization of the beads.

Acknowledgements

The authors would like to acknowledge the financial support of the NIH through Grants R01 DK56890, R01 DK47858, and P41 RR16105, and the support of the National High Magnetic Field Laboratory. The programs tcaCALC and tcaSIM were obtained from the University of Texas Southwestern, and developed through H-47669-16 and RR-02584. NMR data were obtained at the Advanced Magnetic Resonance Imaging and Spectroscopy (AMRIS)

facility of the McKnight Brain Institute of the University of Florida.

References

[1] Soon-Shiong P, Feldman E, Nelson R, Heintz T, Yao Q, Yao Z, et al. Long-term reversal of diabetes by the injection of immunoprotected islets. Proc Natl Acad Sci USA 1993;90:5843–7.

[2] Soon-Shiong P, Heintz RE, Merideth N, Yao QX, Yao Z, Murphy M, et al. Insulin independence in a type 1 diabetic patient after encapsulated islet transplantation. Lancet 1994;343:950–1.

[3] Reach G. Bioartificial pancreas. Diabetic Med 1993;10:105–9.

[4] Lim F, Sun AM. Microencapsulated islets as bioartificial endocrine pancreas. Science 1980;210:908–10.

[5] Lanza RP, Chick WL. Immunoisolation: at a turning point. Immunol Today 1997;18:135–9.

[6] Lanza RP, Chick WL. Transplantation of encapsulated cells and tissues. Surgery 1997;121:1–9.

[7] Benson JP, Papas KK, Constantinidis I, Sambanis A. Towards the development of a bioartificial pancreas: effects of poly L-lysine on alginate beads with βTC3 cells. Cell Transplant 1997;6:395–402.

[8] Constantinidis I, Sambanis A. Towards the development of artificial endocrine tissues: 31P NMR spectroscopic studies of immunoisolated, insulin-secreting AtT-20 cells. Biotechnol Bioeng 1995;47:431–43.

[9] Constantinidis I, Mukundan NE, Gamcsik M, Sambanis A. Towards the development of a bioartificial pancreas: a ^{13}C NMR study on the effect of alginate/poly L-lysine/alginate entrapment on glucose metabolism by βTC3 mouse insulinoma cells. Cell Mol Biol 1997;43:721–9.

[10] Papas KK, Long Jr. RC, Constantinidis I, Sambanis A. Role of ATP and P_i on the mechanism of insulin secretion in the mouse insulinoma βTC3 cell line. Biochem J 1997;326:807–14.

[11] Sambanis A, Papas KK, Flanders PC, Long Jr. RC, Kang H, Constantinidis I. Towards the development of a bioartificial pancreas: immunoisolation and NMR monitoring of mouse insulinomas. Cytotechnology 1994;15:351–63.

[12] Hicks BA, Stein R, Efrat S, Grant S, Hanahan D, Demetriou AA. Transplantation of β cells from transgenic mice into nude athymic diabetic rats restores glucose regulation. Diabetes Res Clin Pract 1991;14:157–64.

[13] Smidsrod O. Molecular basis for some physical properties of alginates in gel state. J Chem Soc Faraday Trans 1974;57:263–74.

[14] Skjak-Braek G, Grasdale H, Smidsrod O. Inhomogeneous polysaccharide ionic gels. Carbohydrate Polym 1989;10:31–54.

[15] Martinsen A, Skjak-Braek G, Smidsrod O. Alginate as immobilization material: I. Correlation between chemical and physical properties of alginate gel beads. Biotechnol Bioeng 1989;33:79–89.

[16] Smidsrod O, Skjak-Braek G. Alginate as immobilization matrix for cells. Trends Biotechnol 1990;8:71–8.

[17] Martinsen A, Storro I, Skjak-Braek G. Alginate as immobilization material: III. Diffusional properties. Biotechnol Bioeng 1992;39:186–94.

[18] Thu B, Bruheim P, Espevik T, Smidsrod O, Soon-Shiong P, Skjak-Braek G. Alginate polycation microcapsules. I. Interaction between alginate and polycation. Biomaterials 1996;17:1031–40.

[19] Thu B, Bruheim P, Espevik T, Smidsrod O, Soon-Shiong P, Skjak-Braek G. Alginate polycation mirocapsules. II. Some functional properties. Biomaterials 1996;17:1069–79.

[20] Constantinidis I, Rask I, Long Jr. RC, Sambanis A. Effects of alginate composition on the metabolic, secretory, and growth characteristics of entrapped βTC3 mouse insulinoma cells. Biomaterials 1999;20:2019–27.

[21] Stabler C, Wilks K, Sambanis A, Constantinidis I. The effects of alginate composition on encapsulated βTC3 cells. Biomaterials 2001;22:1301–10.

[22] Stabler CL, Sambanis A, Constantinidis I. Effects of alginate composition on the growth and overall metabolic activity of betaTC3 cells. Ann NY Acad Sci 2002;961:130–3.

[23] Simpson NE, Stabler CL, Sambanis A, Constantinidis I. The role of the $CaCl_2$–guluronic acid interaction on alginate encapsulated βTC3 cells. Biomaterials 2004;25:2603–10.

[24] Grant GT, Morris ER, Rees DA, Smith PJC, Thom D. Biological interactions between polysaccharides and divalent cations: the egg-box model. FEBS Lett 1973;32:195–8.

[25] Matschinsky FM. A lesson in metabolic regulation inspired by the glucokinase glucose sensor paradigm. Diabetes 1996;45:223–41.

[26] Newgard CB, McGarry JD. Metabolic coupling factors in pancreatic β-cell signal transduction. Annu Rev Biochem 1995;64:689–719.

[27] Prentki M. New insights into pancreatic β-cell metabolic signaling in insulin secretion. Eur J Endocrinol 1996;134:272–86.

[28] Lu DH, Mulder H, Zhao PY, Burgess SC, Jensen MV, Kamzolova S, et al. C-13 NMR isotopomer analysis reveals a connection between pyruvate cycling and glucose-stimulated insulin secretion (GSIS). Proc Natl Acad Sci USA 2002;99:2708–13.

[29] Cline GW, Lepine RL, Papas KK, Kibbey RG, Shulman GI. 13C NMR isotopomer analysis of anaplerotic pathways in INS-1 cells. J Biol Chem 2004;279:44370–5.

[30] Mukundan NE, Flanders PC, Constantinidis I, Papas KK, Sambanis A. Rates of oxygen uptake by free and alginate entrapped βTC3 insulinoma cells. Biochem Biophys Res Commun 1995;210:113–8.

[31] Klokk TI, Melvik JE. Controlling the size of alginate gel beads by use of a high electrostatic potential. J Microencapsul 2002;19:415–24.

[32] Malloy CR, Sherry AD, Jeffrey FMH. Evaluation of carbon flux and substrate selection through alternative pathways involving the citric acid cycle of the heart by ^{13}C-NMR spectroscopy. J Biol Chem 1988;263:6964–71.

[33] Sherry AD, Jeffrey FMH, Malloy CR. Analytical solutions for ^{13}C isotopomer analysis of complex metabolic conditions: substrate oxidation, multiple pyruvate cycles, and gluconeogenesis. Metab Eng 2004;6:12–24.

[34] Simpson NE, Khokhlova N, Oca-Cossio J, Constantinidis I, Insights into the role of anaplerosis in insulin secretion: A ^{13}C NMR study. Diabetologia 2005; submitted for review.

[35] Webb AG, Grant SC. Signal-to-noise and magnetic susceptibility trade-offs in solenoidal microcoils for NMR. J Magn Reson B 1996;113:83–7.

[36] Hsu EW, Schoeniger JS, Bowtell R, Aiken NR, Horsman A, Blackband SJ. A modified imaging sequence for accurate T_2 measurements using NMR microscopy. J Magn Reson B 1995;109:66–9.

[37] Pedersen PL. Tumor mitochondria and the bioenergetics of cancer cells. In: Homburger F, editor. Progress in tumor research, vol. 22. Basel: S. Karger; 1978. p. 190–274.

[38] Sekine N, Cirulli V, Regazzi R, Brown LJ, Gine E, Tamarit-Rodriguez J, et al. Low lactate dehydrogenase and high mitochondrial glycerol phosphate dehydrogenase in pancreatic beta-ells. Potential role in nutrient sensing. J Biol Chem 1994;269:4895–902.

[39] Tziampazis E, Sambanis A. Tissue engineering of a bioartificial pancreas: modeling the cell environment and device function. Biotechnol Progr 1995;11:115–26.

[40] Papas KK, Long Jr. RC, Constantinidis I, Sambanis A. Effects of oxygen on the metabolic and secretory activities of βTC3 monolayers. Biochim Biophys Acta 1996;1291:163–6.

[41] Papas KK, Long Jr. RC, Constantinidis I, Sambanis A. Development of a bioartificial pancreas: II. Effects of oxygen on long-term entrapped bTC3 cell cultures. Biotechnol Bioeng 1999;66:231–7.

[42] Papas KK, Long Jr. RC, Sambanis A, Constantinidis I. Effects of short-term hypoxia on a bioartificial pancreatic construct. Cell Transplant 2000;9:415–22.

[43] Matschinsky FM, Ellerman JE. Metabolism of glucose in the islets of Langerhans. J Biol Chem 1968;243:2730–6.

[44] Malaisse WJ, Sener A, Herchuelz A, Hutton JC. Insulin release: the fuel hypothesis. Metabolism 1979;28:373–85.
[45] Hildebrandt P, Sejrsen P, Nielsen SL, Birch K, Sestoft L. Diffusion and polymerization determines the insulin absorption from subcutaneous tissue in diabetic patients. Scand J Clin Lab Invest 1985; 45:685–90.
[46] Sakai S, Ono T, Ijima H, Kawakami K. In vitro and in vivo evaluation of alginate/sol–gel synthesized aminopropyl-silicate/alginate membrane for bioartificial pancreas. Biomaterials 2002;23: 4177–83.
[47] Papas KK, Long Jr. RC, Constantinidis I, Sambanis A. Development of a bioartificial pancreas: I. Long-term propagation and basal and induced secretion from entrapped bTC3 cell cultures. Biotechnol Bioeng 1999;66:219–30.
[48] Sutherland RM. Cell and environment interactions in tumor microregions: the multicell spheroid model. Science 1988;240: 177–84.
[49] Sillerud LO, Freyer JP, Neeman M, Mattingly MA. Proton NMR microscopy of multicellular tumor spheroid morphology. Magn Reson Med 1990;16:380–9.
[50] MacDonald MJ, Fahien LA, Brown LJ, Hasan NM, Buss JD, Kendrick MA. Perspective: emerging evidence for signaling roles of mitochondrial anaplerotic products in insulin secretion. Am J Physiol Endocrinol Metab 2005;288:E1–E15.